AIAA JOURNAL
Vol. 40, No. 6, June 2002

Particle Image Velocimetry in Mach 3.5 and 4.5 Shock-Tunnel Flows

J. Haertig,* M. Havermann,† C. Rey,‡ and A. George§
French–German Research Institute of Saint-Louis, 68301 Saint-Louis, France

For the first time, a particle image velocimetry (PIV) system was used to study high-Mach-number flows in a shock-tunnel facility with velocities of more than 1.5 km/s and measuring times in the millisecond range. An application of PIV to such a transient high-speed flow is considerably more difficult than to a continuous flow because no online adjustments of the optics and the particle seeding can be done. Additionally, a proper seeding and timing of the facility is crucial. First we will discuss the measured velocity field behind a contoured Laval nozzle (design Mach number 4.5). The measurement data show that the flowfield at the nozzle exit is parallel to the nozzle axis and homogeneous as expected from supersonic nozzle theory. The average measured velocity corresponds very well to the calculated flow velocity. The results are compared to measurements made with a conical Mach 3.5 nozzle that exhibits a diverging flowfield. A wedge was further introduced into the parallel Mach 4.5 nozzle flow to study the seed particle performance downstream of an oblique shock. The measured results are also in good agreement with calculated velocities from oblique shock theory. PIV has, therefore, proven to be an efficient measurement method for high-speed and short-duration simulation facilities.

Introduction

PARTICLE image velocimetry (PIV) has gained an important role in modern flowfield diagnostics during the past decade.[1] Concerning supersonic flows, PIV systems have been used to measure flow velocities in supersonic blow-down wind tunnels at the French–German Research Institute of Saint-Louis (ISL).[2,3] Humphreys et al. used PIV at the NASA Langley Research Center hypersonic blowdown tunnel to measure a Mach 6 flowfield with velocities up to 930 m/s (Refs. 4 and 5). Lang applied PIV to study the vortex flow around a delta wing at a freestream Mach number of 2 in the trisonic blowdown wind tunnel of the Aerodynamisches Institut Aachen in Germany.[6,7] Ünalmis et al. applied PIV to measure velocity fluctuations in a boundary layer at a freestream Mach number of 5 (velocity of 765 m/s) in the supersonic blowdown wind tunnel of the University of Texas at Austin.[8] Supersonic freejets of nominal Mach numbers up to 3 were studied by several authors (for example, Yüceil et al.[9] and Alkislar et al.[10]).

Because of the low-stagnation states, the static temperature and pressure of blowdown facility flows do not correspond to real flight conditions in the lower atmosphere. To get real flow conditions for lower atmospheric flight at even higher Mach numbers, it is convenient and economical to use a shock-tunnel facility. Its main disadvantage is the short measuring time, which is of the order of milliseconds. Because the preparations for one experiment require several hours of work and a considerable amount of gas, a high information density for each experiment is desirable. The PIV technique allows an instantaneous and two-dimensional measurement of the velocity field. For these reasons it was tested at the ISL shock tunnel.

ISL Shock-Tunnel Facility

A shock tunnel is a short-time-duration wind-tunnel facility consisting of a shock tube with a supersonic nozzle (Fig. 1). The nozzle exit is connected to a test chamber with optical access from three sides. The test chamber opens into a dump tank for catching the shock-tube gases. The ISL shock tube has an inner diameter of 100 mm and is divided into a 2.7-m-long, high-pressure driver tube and a 18.4-m-long, low-pressure driven tube. The driver gas consists of a mixture of hydrogen and nitrogen at a pressure of up to 50 MPa, whereas the driven or test gas consists of pure nitrogen at a pressure of up to 0.5 MPa. The two sections containing the stagnant gas are separated by a steel diaphragm (thickness up to 4 mm) before the experiment starts. The shock-tube operation is explained in the following and can well be illustrated by a wave diagram (Fig. 2). After the diaphragm bursts, a left-traveling rarefaction wave propagates into the high-pressure gas, and a right-traveling shock wave propagates at a supersonic speed (typically 1000 m/s) into the low-pressure test gas. The interface between the driver and the test gas is called the contact line; it moves behind the shock wave at a slower speed. The test gas behind the shock wave is accelerated, and its temperature and pressure rise according to the one-dimensional shock theory. The shock tunnel can be operated either with or without shock reflection depending on the nozzle design used.

For the first case, a convergent–divergent nozzle with a throat (Laval nozzle) is used. The moving shock wave is reflected at the beginning of the convergent entrance section of the nozzle, which coincides with the end of the driven tube. The shock travels back through the accelerated test gas, brings it nearly to rest, and further increases the test gas pressure and temperature. Thereby a highly compressed and heated quiescent gas volume with a pressure of up to 25 MPa and a temperature of about 1300 K is produced. These conditions determine the stagnation conditions of the nozzle. The duration of the stagnation state of the flow is maximized if the returning shock wave crosses the arriving contact line without producing a reflected shock or expansion wave at the interface (tailored interface conditions). Then the test time is limited by the arrival of the expansion waves that were produced in the driven-tube section at the diaphragm burst and that were reflected at the high-pressure end wall. It is normally necessary to use a mixture of gases in the driver tube to obtain such tailored interface conditions; here a fraction of 13% nitrogen is mixed with hydrogen.

In the case of the nonreflection operation of the shock tunnel, a divergent nozzle without throat (full-capture nozzle) is attached to the end of the driven tube. The shock wave first accelerates and compresses the test gas and then travels through the nozzle into the dump tank. The test gas following the shock must have been accelerated to a supersonic speed before entering the divergent nozzle to be further accelerated to a higher supersonic speed in the nozzle. In this case, the test time is either limited by the arrival of the expansion fan or

Presented as Paper 2001-0699 at the AIAA 39th Aerospace Sciences Meeting, Reno, NV, 8–11 January 2001; received 5 March 2001; revision received 9 October 2001; accepted for publication 19 October 2001.

*Research Scientist, Department of Aerodynamics and Ballistics, 5 Rue du Général Cassagnou. Member AIAA.
†Research Scientist, Shock Tube Department, 5 Rue du Général Cassagnou.
‡Engineer, Department of Aerodynamics and Ballistics, 5 Rue du Général Cassagnou.
§Engineer, Shock Tube Department, 5 Rue du Général Cassagnou.

Table 1 Freestream flow conditions in the shock tunnel flow for nitrogen at a Mach number of 4.5

Flow condition	Atmospheric height, km	Static pressure, kPa	Static temperature, K	Density, kg/m^3
1	2.5	77	270	0.96
2	5.5	50	252	0.70
3	8.5	33	235	0.47

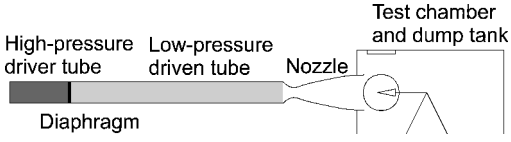

Fig. 1 ISL shock-tunnel facility.

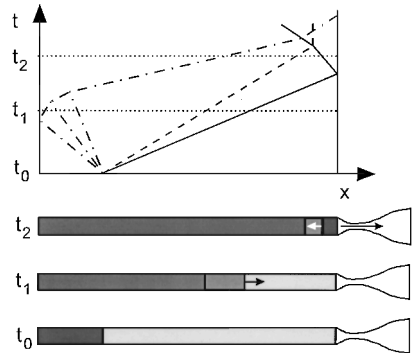

Fig. 2 Wave diagram of shock-tube operation: ——, shock wave; –·–, rarefaction wave; and – – –, contact line.

the arrival of the contact line followed by the driver gas, whatever occurs first.

For both modes of shock-tunnel operation, the measuring time is of the order of 1–2 ms. These values were both calculated and determined experimentally by means of pitot tube measurements.

The advantage of a full-capture nozzle compared to a Laval nozzle is that it is easier to manufacture and that it has a larger exit diameter for a given Mach number. On the other hand, the nonreflection mode requires a considerably higher driver pressure than the reflection-mode operation. Therefore, it is convenient to use a full-capture nozzle for lower Mach numbers and a Laval nozzle for higher Mach numbers.

The stagnation conditions for both modes of operation are accurately recalculated for each run using the measured shock-wave speed in the driven tube because the diaphragm burst pressure varies slightly from shot to shot.

In the shock-reflection mode, a contoured Laval nozzle (throat diameter of 50 mm, exit diameter of 220 mm) is used here. The flow is accelerated to a Mach number of 4.5 at the nozzle exit, and a parallel freestream is produced. The freestream pressure and temperature can be adjusted by varying the driver and driven gas pressures to match real atmospheric conditions at heights between 2.5 and 8.5 km above sea level (Table 1). Because of the simulated temperature variation at these heights, a Mach number of 4.5 corresponds to flow velocities between 1500 and 1400 m/s for the nitrogen test gas, respectively. Alternatively, a conical full-capture Mach 3.5 nozzle without shock reflection can be used.

The nozzle exit diameter is 250 mm, and the cone half-angle is 8.5 deg, so that a slightly diverging flow can be expected to occur. A Mach number of 3.5 corresponds to flow velocities between 1170 and 1090 m/s for the mentioned atmospheric conditions, respectively.

PIV Velocity Measurements

To measure the freestream flow velocity a PIV system was installed at the shock tunnel (Fig. 3). The velocities of more than 1 km/s encountered in this flow imposed the use of a double-pulse laser system with a pulse separation time in the microsecond range. For this purpose, two frequency-doubled Nd-YAG-lasers (Quantel

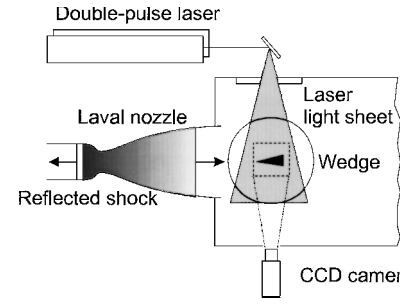

Fig. 3 PIV system mounted at the ISL shock-tunnel facility.

Twins) with a pulse energy of 150 mJ each were used in combination with a synchronizer. The pulse separation was checked with a high-speed photodiode (5 ns rise time) connected to a 200-MHz digital oscilloscope (Tektronix TDS 420 A). No timing errors relative to the synchronizer settings could be detected. Triggering of the synchronizer was accomplished by a fast-response heat flux probe mounted in the driven-tube wall. The probe detects the arrival of the shock wave propagating in the tube, and an electronic delay circuit triggers the lasers exactly at the point when the flow is quasi-stationary at the nozzle exit.

A laser light sheet (0.2 mm thick, 300 mm wide) perpendicular to the nozzle axis was created by means of a telescope and reflected vertically into the test section. The imaging charge-coupled device (CCD) camera (TSI PIVcam, 1000 × 1016 pixels, pixel size 9 × 9 μm) is capable of acquiring two images within a pulse delay in the microsecond range. It was mounted on the horizontal axis to view the illuminated flowfield behind the nozzle exit. Different Nikon camera objectives were mounted to the CCD camera to change the field of view. The image data were analyzed after each run with a cross-correlation technique using the TSI Insight 2.0 software. The correlation window was set to 64 × 64 pixels with a 50% overlap shifting during the analysis. With these settings, the percent of valid vectors was in the range of 95–98%. Because timing errors of the Nd:YAG laser could be excluded, the velocity measurement accuracy depends on the correlation peak estimation error. A typical value is ±0.1 pixel for the algorithms used by the TSI software.

TiO_2 particles were used to seed the test gas in the driven tube before the experiment was triggered. The nominal particle diameter d_p given by the supplier was 0.32 μm. An electron microscopy analysis yielded a mean diameter of about 0.4 μm, however. For this diameter, the theoretical particle relaxation time τ was calculated with Eq. (1) (Ref. 11, p. 293) to 2.1 μs:

$$\tau = \rho_p d_p^2 \big/ 18\mu \tag{1}$$

Particle density $\rho_p = 4200$ kg/m^3 (Ref. 11, p. 305), and the coefficient of viscosity for nitrogen at 293 K is $\mu = 1.8 \times 10^{-5}$ kg/m · s. The particles were injected simultaneously with the nitrogen test gas into the driven tube by means of a fluidized-bed seeder. To avoid larger agglomerated TiO_2 particles entering the tube, a cyclone separator controlled the size distribution of the particles, allowing only smaller particles to pass. The seeding density of TiO_2 was optimized by several preliminary experiments, and good results were obtained for a mass ratio (particles/gas) of approximately 0.15%, which corresponded to a theoretical seeding density of about 10,000 particles/mm^3 in the driven tube before the shot. Approximately 10–20 particles were present per interrogation window. However, the particle density varied considerably due to the strong density gradients in the flow.

Experimental Results

Mach 4.5 Nozzle Flow

Three freestream conditions corresponding to atmospheric conditions at heights of 2.5, 5.5, and 8.5 km were studied for the reflected mode Mach 4.5 Laval nozzle (flow condition numbers 1, 2, and 3, respectively). The nozzle exit velocities were measured by PIV and compared to calculated values obtained from a one-dimensional shock-tube/nozzle code, which took into account real gas effects. The PIV system recorded two images with a pulse delay of 1.5 μs,

Table 2 Calculated and measured (PIV) velocities of the nozzle flow

Flow condition	Mach number	Calculated velocity, m/s	Average measured velocity, m/s	Difference measurement calculation, %
1	4.5	1510.8	1519.1 ± 14.4	+0.5
2	4.5	1455.1	1439.7 ± 17.0	−1.1
3	4.5	1414.2	1424.6 ± 15.3	+0.7

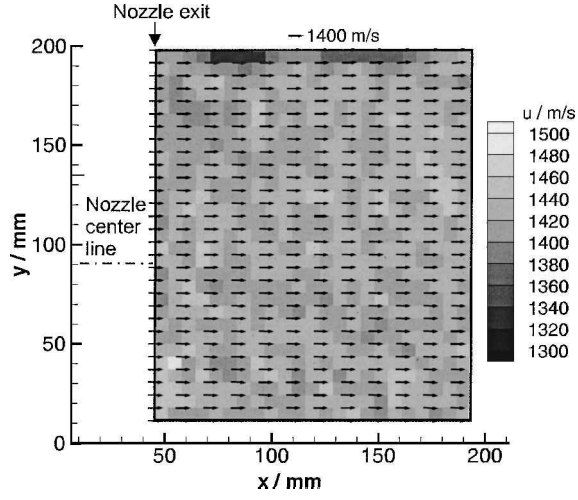

Fig. 4 PIV measurement of the horizontal flow velocity behind the Mach 4.5 Laval nozzle (flow condition 2).

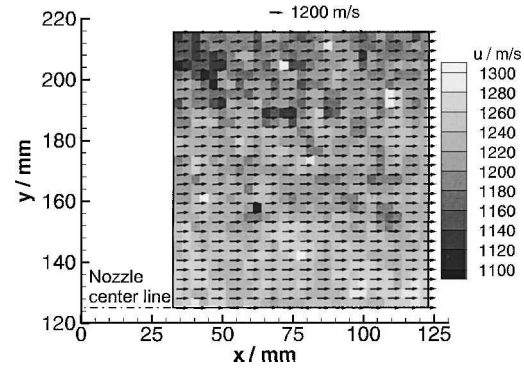

Fig. 5 Horizontal flow velocity component of the conical Mach 3.5 nozzle (nozzle exit at $x = 0$ mm).

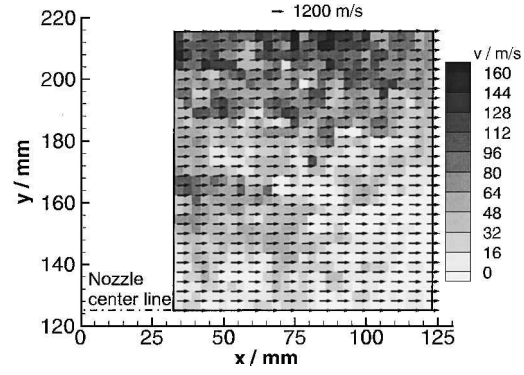

Fig. 6 Vertical flow velocity component of the conical Mach 3.5 nozzle (nozzle exit at $x = 0$ mm).

and the field of view was 200 × 200 mm using a camera lens focal length of 50 mm and an aperture of f-4. The optical system calibration factor was determined to 201 μm/pixel so that a maximum particle displacement of about 11 pixels could be expected for a velocity of 1500 m/s. The spatial resolution was estimated to 32 × 32 pixel (=6.4 × 6.4 mm) corresponding to the 50% overlap of the correlation window size. The cross correlation performed by the TSI software yielded the two-dimensional velocity distribution of the imaged flowfield, which is shown in Fig. 4 for the horizontal velocity component u (condition 2). The results show a rather homogeneous flowfield in the center of the nozzle flow. In the upper part, the horizontal flow velocity is lower because the flow is underexpanded and slightly diverged at the nozzle tip.

The data for all flow conditions studied are summarized in Table 2, and it can be seen that the average measured velocity is very close to the calculated velocity. The relative standard deviation for all cases is about ±1%, which is comparable to the correlation peak estimation error of ±0.1 pixel (= ±13.4 m/s) of the cross-correlation software.

Mach 3.5 Nozzle Flow

The conical full-capture nozzle has an exit diameter of 250 mm and a nominal exit Mach number of 3.5. Because of the conical nozzle shape with a constant divergence angle of 8.5 deg, the flowfield cannot be expected to be as homogeneous and parallel as the flowfield of a contoured Laval nozzle. It is, therefore, difficult to predict the velocity field downstream from the nozzle exit using one-dimensional theory.

The nozzle flow was measured by PIV only for one flow condition, corresponding to 2.5-km height. A field of view of about 90 × 90 mm lying above the axis of symmetry was imaged on the CCD array using a camera lens focal length of 105 mm with an aperture of f-11. The f-number was increased because the laser light sheet width was reduced to 200 mm for this experiment. The optical system calibration factor was measured to 97.6 μm/pixel so that the pulse separation time had to be lowered to 0.8 μs to obtain a maximum particle displacement of about 10.6 pixels for a flow velocity of 1300 m/s. The spatial resolution corresponding to the 32 × 32 pixel overlap window size was estimated to 3.1 × 3.1 mm.

The measured horizontal and vertical velocity components are shown in Figs. 5 and 6, respectively. Both components show a nonuniform and divergent flowfield. The horizontal velocity component is decelerated with increasing radial distance from the centerline, whereas the vertical velocity component is accelerated.

It is remarkable that the measured mean velocity range of 1250 m/s along the nozzle centerline is higher than the theoretically predicted velocity of 1170 m/s at the nozzle exit. The velocity measurement accuracy was estimated to ±12.2 m/s, corresponding to ±0.1 pixel.

Mach 4.5 Wedge Flow

To study particle lag effects, some experiments were conducted using the Mach 4.5 Laval nozzle and a wedge (half-angle 10 deg). In supersonic flow, an oblique shock wave occurs at the wedge tip, where the flow is turned in parallel with the wedge surface. The shock-wave angle is a function of both the Mach number and the wedge angle and can be calculated according to the gasdynamic equations.

To increase the spatial resolution, the field of view of the CCD camera was reduced to 84 × 84 mm (camera lens focal length of 105 mm/f-2.5), and the laser pulse separation was further reduced to 0.6 μs. With the measured optical system calibration factor of 84.2 μm/pixel, a maximum particle displacement of 10.7 pixels was calculated for a flow velocity of 1500 m/s. The 32 × 32 pixel overlap window size resulted in a spatial resolution of 2.7 × 2.7 mm.

The PIVcam picture in Fig. 7 shows the particle distribution in the flow over the wedge. The particle distribution is very homogeneous, and the density jump across the shock can be clearly seen. The measured shock wave angle of about 20 deg coincides with the theoretical value for a Mach number of 4.5. Figures 8 and 9 show the measured horizontal and vertical flow velocity distribution for flow condition 2. The shock wave can be clearly distinguished in the PIV measurements. The mean value for the horizontal and vertical velocity components of all correlation windows inside the shock was calculated. A comparison between these measurements and the predicted velocities is given in Table 3, and a good agreement between theory and experiment can be observed. The standard deviations are close to the velocity measurement accuracy (±0.1 pixel = ±14 m/s).

Table 3 Calculated and measured freestream velocity before the shock and horizontal u and vertical v velocities of the flow over a wedge after the shock

	Before shock		After shock			
Flow condition	Calculated velocity, m/s	Measured velocity, m/s	Calculated velocity u, m/s	Measured velocity u, m/s	Calculated velocity v, m/s	Measured velocity v, m/s
1	1518.0	1498.7 ± 28.5	1424.1	1416.0 ± 10.3	251.1	249.7 ± 19.0
2	1453.7	1446.5 ± 10.6	1364.3	1331.0 ± 9.3	240.6	234.7 ± 12.6
3	1434.9	1433.1 ± 10.8	1346.7	1331.9 ± 10.1	237.5	234.8 ± 22.6

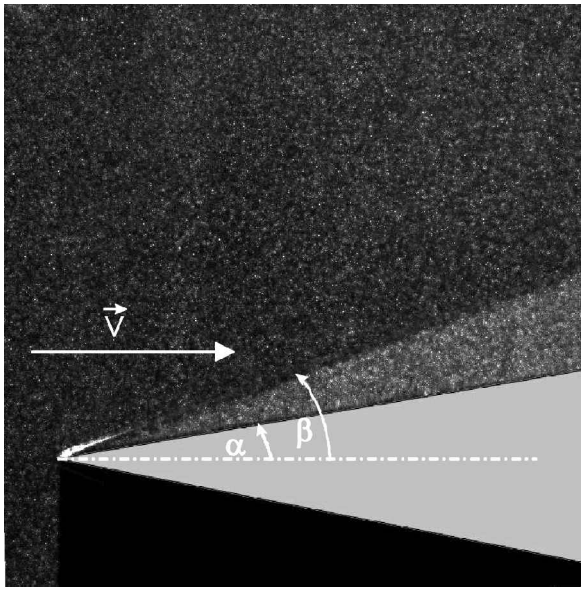

Fig. 7 PIVcam picture of the flow over a wedge with wedge half-angle of $\alpha = 10$ deg; shock-wave angle β can be measured from this picture.

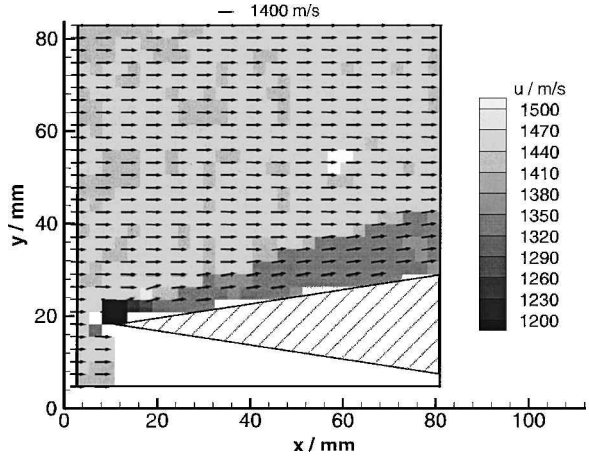

Fig. 8 PIV measurement of horizontal flow velocity of wedge flow (flow condition 2).

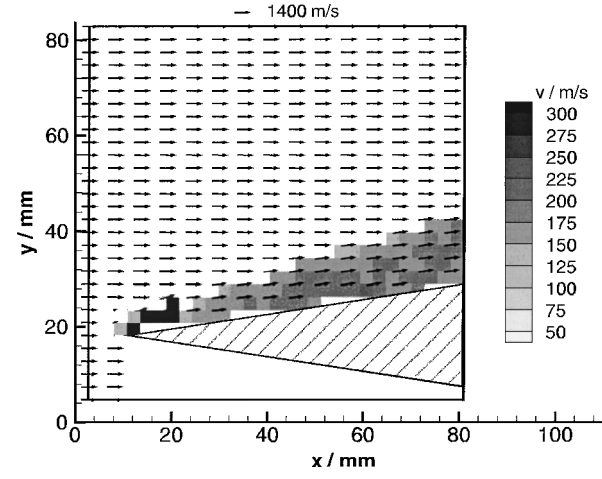

Fig. 9 PIV measurement of vertical flow velocity of wedge flow (flow condition 2).

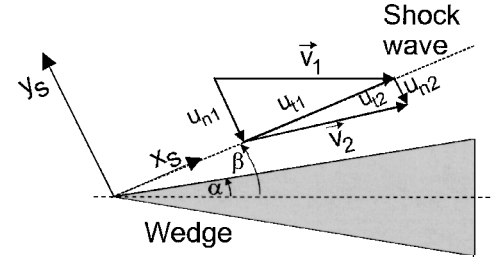

Fig. 10 Oblique shock at a wedge; shock wave coordinate system (x_s–y_s) and corresponding velocity vector decomposition (u_t–u_n, respectively).

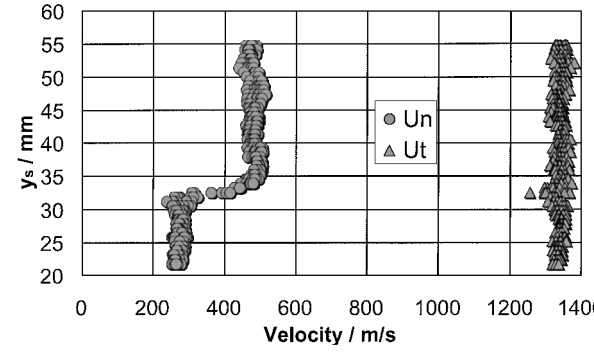

Fig. 11 Normal and tangential velocity lines with respect to the oblique shock.

Seed Particle Performance

The seed particle performance is important for all particle-based laser measurement systems such as laser Doppler velocimetry, global Doppler velocimetry, and PIV.[12] For high-quality measurements, the particle lag should be small compared to the geometrical scale of the model. The efficiency of the seed particles can be studied from wedge flow measurements using the oblique shock theory. The velocity vector $\boldsymbol{v}$ can be split in a normal, u_n, and a tangential component u_t with respect to the shock wave (Fig. 10). The tangential component of the flow velocity is preserved across an oblique shock wave, and for the normal velocity component the relations for a normal shock can be applied. The acquired PIV images of the wedge flow were first rotated with the angle of the shock wave β and then reanalyzed. Several lines perpendicular to the shock wave were chosen, and both the perpendicular and parallel velocity distribution with respect to the shock are plotted in Fig. 11. They show that the normal velocity component is decelerated within a distance of about 3 mm. The calculated relaxation distance using a particle's relaxation constant of 2.1 μs and the standard Stokes law for sphere drag was calculated to 2 mm. The difference can be explained by agglomeration of TiO_2 and by the limited spatial resolution of the PIV correlation method.

The tangential velocity component remains unchanged across the shock wave as expected by theory. These results confirm the efficiency of the PIV measurements and show that particle lag effects are within the spatial resolution of the system. To improve the spatial resolution, it is planned to use a more sophisticated software incorporating a high-resolution mesh-free algorithm for the PIV image processing.[13]

Conclusions

A PIV system was used at the ISL shock tunnel to measure high-speed velocity fields. First, the flowfields of a Mach 4.5 contoured Laval nozzle and a Mach 3.5 conical nozzle were measured and compared. The flowfield of the Mach 4.5 nozzle was homogeneous as expected from theory, whereas the flowfield of the conical nozzle exhibited a flow divergence. It was found that the measured freestream conditions of the Mach 3.5 conical nozzle did not correspond to the theoretical one-dimensional nozzle exit conditions.

The measured velocities for the Mach 4.5 nozzle seem to be the highest measured by PIV to date. The velocity range was slightly varied between 1425 and 1519 m/s by changing the stagnation conditions in the shock tube.

The parallel Mach 4.5 flow was further used to produce a two-dimensional flow over a wedge. This kind of flow is ideally suited to study the seed particle performance. It was shown that the flow over a wedge also agreed very well with calculated velocities. The particle relaxation length was found to be of the same order of magnitude as the size of one correlation window.

The PIV method has, therefore, proven to work efficiently and accurately in high-speed shock-tunnel flows for the first time. Because PIV is a planar technique that yields two-dimensional quantitative results, it is ideally suited to be compared to numerical calculations. Therefore, it is planned to use the PIV method in the ISL shock tunnel to study more complex flows such as flow–lateral jet interactions, shock formation across spiked models, and nozzle flow performance. However, for this purpose the spatial resolution must be increased. The spatial resolution is primarily limited by the correlation window, which in turn depends on the particle displacement. Therefore, for high-speed applications the laser pulse delay must be reduced further, which requires the use of an improved CCD camera.

References

[1]Raffel, M., Willert, C. E., and Kompenhans, J., "Introduction," *Particle Image Velocimetry: A Practical Guide*, Springer-Verlag, Berlin, 1998, pp. 1–12.

[2]Haertig, J., and Smigielski, P., "Light Sheet Visualization and Velocity Measurements in Seeded Flows," *Proceedings of the Third International Symposium on Applications of Laser Anemometry to Fluid Mechanics*, Calouste Gulbenkian Foundation, Lisbon, 1986, Paper 19.2.

[3]Johé, C., Duffner, P., Haertig, J., and Demeautis, C., "PIV: Validation en Écoulement Subsonique et Supersonique," *Proceedings of the 5^e Congrès Francophone de Vélocimetrie Laser*, Complexe de Recherche Interprofessionnel en Aérothermochimie, Université et Institut National des Sciences Appliquées de Rouen, Rouen, France, 1996, Paper I.1.

[4]Humphreys, W. M., Rallo, R. A., Hunter, W. W., and Bartram, S. M., "Application of Particle Image Velocimetry to Mach 6 Flows," *Proceedings of the 5th International Conference of Laser Anemometry, Advances and Applications*, Vol. 2052, International Society for Optical Engineering (SPIE), Veldhoven, The Netherlands, 1993, pp. 519–526.

[5]Humphreys, W. M., Bartram, S. M., and Blackshire, J. L., "A Survey of Particle Image Velocimetry in Langley Aerospace Facilities," AIAA Paper 93-0411, Jan. 1993.

[6]Lang, N., "PIV Measurements in Sub- and Supersonic Flow over the Delta Wing Configuration ELAC," *Proceedings of the 8th International Symposium on Flow Visualization*, Università degli Studi di Napoli Federico II, Sorrento, Italy, 1998, Paper 205.

[7]Lang, N., "Investigation of the Supersonic Flow Field Around a Delta Wing Using Particle Image Velocimetry," *Proceedings of the 10th International Symposium on Applications of Laser Anemometry to Fluid Mechanics*, Calouste Gulbenkian Foundation, Lisbon, 2000, Paper 4.3.

[8]Ünalmis, Ö. H., Hou, Y. X., Bueno, P. C., Clemens, N. T., and Dolling, D. S., "PIV Investigation of Role of Boundary Layer Velocity Fluctuations in Unsteady Shock-Induced Separation," AIAA Paper 2000-2450, June 2000.

[9]Yüceil, K. B., Ötügen, M. V., and Arik, E., "Underexpanded Sonic Jets: A PIV Study," *Proceedings of the 10th International Symposium on Applications of Laser Anemometry to Fluid Mechanics*, Calouste Gulbenkian Foundation, Lisbon, 2000, Paper 8.6.

[10]Alkislar, M. B., Lourenço, L. M., and Krothapalli, A., "Stereoscopic PIV Measurements of a Screeching Supersonic Jet," *Journal of Visualization*, Vol. 3, No. 2, 2000, pp. 135–143.

[11]Durst, F., Melling, A., and Whitelaw, J. H., *Principles and Practice of Laser-Doppler Anemometry*, 2nd ed., Academic Press, London, 1981.

[12]Haertig, J., and Fleck, V., "Anemométrie Laser, Amélioration de la Précision des Mesures par Élimination des Erreurs dues à la Présence de Grosses Particules," French–German Research Inst. of Saint-Louis, ISL Rept. 10/74, Saint-Louis, France, 1974.

[13]Lourenço, L. M., and Krothapalli, A., "TRUE Resolution PIV: A Mesh-Free Second Order-Accurate Algorithm," *Proceedings of the 10th International Symposium on Applications of Laser Anemometry to Fluid Mechanics*, Calouste Gulbenkian Foundation, Lisbon, 2000, Paper 13.5.

W. R. Lempert
Guest Associate Editor